The use of the D+ solution in magnetotelluric interpretation

D. Beamish[a] and J.M. Travassos[b]

[a] *British Geological Survey, Keyworth. Nottingham NG 12 5GG, UK*

[b] *Departamento de Geophysica, CNPq-Observatorio Nacional. R. Gen. Bruce 586, 20291 Rio de Janeiro. Brazil*

Beamish, D. and Travassos, J.M., 1992. The use of the D + solution in magnetotelluric interpretation. Journal of Applied Geophysics, 29, 1-19.

ABSTRACT

The MT interpretation procedure begins with a set of sounding data in the frequency domain. The overall quality of these data can be variable both as a function of frequency and location. Many simple interpretation procedures, such as the assessment of static distortion, act directly on the sounding data. A number of response characteristics, such as the location (in frequency) and number of turning points, are important to the interpretation. Localised scatter (noise) in the response estimates can produce false gradients which degrade the quality of the inferences made from the data.

This study considers how the D+ solution can be used to process the raw sounding data to provide a number of interpretational advantages. Although the D+ solution has strict formal roots in I D inverse theory, it is used here simply to enhance those data attributes, particularly that of physical validity, which lead to a more meaningful assessment of data characteristics. The data considered are 84 broadband array soundings from the Parana basin, Brazil. The advantages provided by the D+ processed data set are demonstrated by using the raw and processed data in two main interpretational procedures. The first procedure concerns the ability of the data to provide quantitative assessments of the influence of static distortion. The second procedure concerns the application of transform methods which attempt to recover a resistivity *I* depth or reflectivity profile directly from the sounding data.

Introduction

In the magnetotelluric (MT) method the interpretation procedure begins with a data set consisting of one or more sounding curves (response functions) in the frequency domain. Normally the sounding data will be a complex response expressed as apparent resistivity (ρ_a) and (φ). It is not our intention here to consider the subject of the various techniques which may be used for reliable MT response function estimation. A recent review is provided by Jones et al. (1989). The overall quality of an MT data set obviously depends on the specific field system and processing methods used but it also depends, more generally, on the signal/ noise environment and can often be a function of acquisition time and therefore cost.

When the sounding data are first examined it is usually the case that the first "rule" of assessment, that of physical validity, is not fully addressed. The physical validity of a smooth response appears as a "background concept" in a good deal of work which deals with the processing and interpretation of MT data. It should be recognised that "final" processed data may have been subjected to sensible but somewhat ad-hoc procedures. Such processing procedures often use the necessary condition of frequency stability of a "correct" response to reject or suppress outliers. Such procedures may be applied during time-series processing (Young and Kitchen, 1989) or during initial "data editing" of response values (Morrison et al., 1990). Other schemes involve smoothing and interpolation to resample the response. (Jiracek et al., 1989) or smoothing while imposing a requirement that the data exhibit minimum-phase behaviour (Tzanis and Beamish, 1989; Park et al., 1991).

In a formal sense, the subject of assessing tensor sounding data for physical validity is quite complex. For data which are scalar (one-dimensional, 1D), a set in inequality constraints have been established (Weidelt, 1972, 1986) which must be upheld by a valid response function. The formalism for validity when dealing with data of higher order is less satisfactory. According to Park et al. (1991), minimum-phase behaviour of the MT response is predicted for 1D and 20 structures but has not been verified for 30 structures. Dispersion relationships also exist which connect the real and imaginary parts of the response and (ρ_a,φ). (Weidelt, 1972; Fischer and Schnegg, 1980). Parker (1983) notes, however, that such types of relationship offer only weak constraints on data validity and indicates that the most powerful method for ensuring a physically valid response is obtained by extracting and examining a fundamental class of model solution called DPLUS (D+).It is clear from the above considerations that, at present, the practical problem of assessing the physical validity of a response is only tractable for the 1D case.

From a physical point of view, when the underlying principles of causality and passivity are applied to the field relationships, the necessary smooth behaviour of the response function can be established. As indicated above, even a cursory examination of published response data reveals that many soundings contain scattered estimates (localised in frequency) over certain portions of the bandwidth. It is unreasonable to suggest that such behaviour can be attributed to high-order dimensional effects since this would imply that the free-current decay exhibited resonances, often at a single frequency. It is more reasonable to suggest that much of the observed scatter is due to our less-than-perfect measurement and estimation schemes. High-order and unphysical scatter in the

original data introduces noise into many of the methods that are used for preliminary interpretation. Such noise contamination becomes particularly acute in methods which require the first or second-order derivatives of the response to be estimated.

The data considered in this study are 84 broadband (100 to 0.001 Hz) grid array soundings from the Parana basin, Brazil. A broad location map is given in Fig. 1. An examination of these soundings reveals data which contain unphysical scatter in various degrees, and which are otherwise 1D but are contaminated with the classic characteristics of static distortion. The present study largely concerns the problem of reducing the unphysical data attributes in order to improve data interpretation. In order to do this a consideration of "dimensional" data attributes, including the influence of static distortion, is also required but is secondary to the main aim.

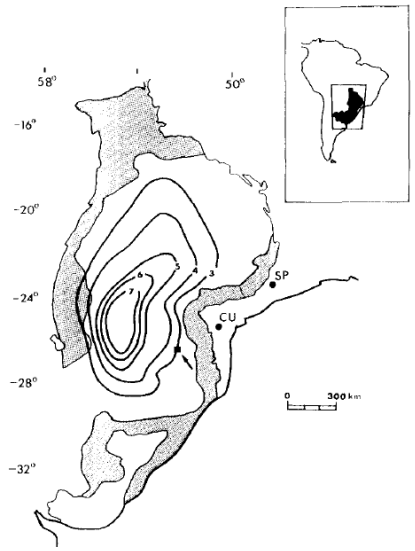

Figure 1. Main location map. Parana basin outlined on inset map of South America. Main map shows extent of basalt cover (unshaded) and structural contours of depth to seismic basement (after Zalan et al., 1986). Contour interval I km. Shaded region is sedimentary outcrop. Position of Clevelandia MT array is indicated by the solid square (arrowed). *SP*= Sao Paulo, CU= Curitiba.

A brief background to the D+ solution due to Parker (1980) and Parker and Whaler (1981) is given. For the data set considered, adequate o+ solutions misfits can be obtained for the vast majority of soundings. Although the D+ solution *models* (which comprise delta functions with depth) are difficult to interpret directly, the D+ solutions can be used to reconstruct an effectively continuous response function. The response function obtained is physically valid and provides an important set of smoothing, interpolation and extrapolation properties. Processing the entire data set in this way results in a "homogenous" data set which provides significant advantages in many of the subsequent processing procedures that can be applied to array data.

The advantages provided by the D+ processed data set are demonstrated by using the raw and processed data in two main interpretational procedures. The first procedure concerns the ability of the data to provide both qualitative and quantitative assessments of the influence of static distortion. The second procedure concerns the application of simple transform methods which attempt to recover a resistivity/depth profile directly from the sounding data.

The MT array data

The data discussed here were acquired and processed by a commercial contractor in the early 1980's. Some of the background to MT measurements in the Parana basin is discussed by Stanley et al. (1985) who report on a regional MT survey (8 to 15 km site spacing) conducted further north in the region of a major linear uplift (the Ponta Grossa arch). The present data, referred to by locality, as Clevelandia, were collected as a detailed grid survey (about 2 km site spacing) in the vicinity of a deep stratigraphic drill hole. The main location map is shown in Fig. 1 and the map shown in Fig. 2 gives the location of the 84 sounding sites whose data are discussed. Six approximately east-west lines, each containing between 13 and 15 sites, are shown arrowed in Fig. 2.

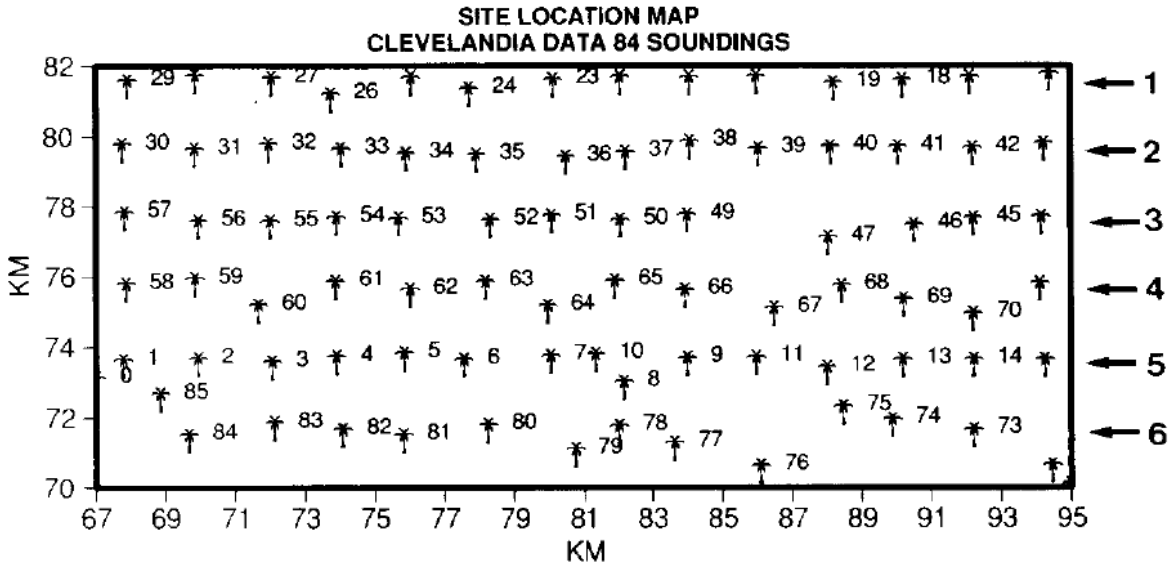

Figure 2. MT sounding locations of the Clevelandia grid array. No data exists for site 48. Positions of 6 approximately east-west lines (referred to in the text) are shown arrowed.

Although geological interpretation is not the aim of this study, a few relevant aspects should be noted. The Palaeozoic sediments of the Parana basin are covered by the world's most extensive flood basalt complex (Zalan et al., 1986). The 1 to 2 km thick basalts Mid- to Early Cretaceous) cover an area of over 800,000 km^2 (see Fig. 1) and have hampered geophysical basin evaluation. The basin comprises a sequence of conductive (3 to 12 Ω·m) marine and continental sediments. The pre-Devonian basement varies in places from crystalline rock to metasedimentary sequences. Deep well logs indicate that the crystalline basement rocks are consistently resistive (> 100 Ω ·m) but the resistivities of the meta-sedimentary formations are more variable. An important aspect of data interpretation is the possible occurrence of diabase intrusives in the form of dykes, dyke swarms and sills.

The data made available for the present study do not comprise the complete MT tensor. The data were digitised from paper (graph) records and only the main off-diagonal tensor elements *(ρ_{xy} , φ_{xy}; ρ_{yx} , φ_{yx})* are available for analysis. This means that no rotational characteristics or tensor decompositions can be extracted from the sounding data. This is not too restrictive in preliminary data interpretation since initial assessments of data characteristics are often made using only the two observed (unrotated) off-diagonal elements. In addition, when the data are to be assessed for static distortion effects the data characteristics in the measured (unrotated) coordinate frame are

required. This is because a general distortion tensor, at a given site, may operate on the two electric field components either individually or in combination and "correct" tensor rotation or decomposition assumes prior knowledge of the individual distortion elements.

An example of the type of data obtained across the array is shown in Fig. 3. The 15 sounding curves and standard errors in the *XY* component from line 5 (Fig. 2) are shown superimposed. The sounding bandwidth covers 5 decades from slightly over 100 Hz to about 0.001 Hz. A broadly homogenous frequency response is observed and, although it is not very clear in this presentation (see later examples), individual response curves are sampled non-uniformly along the frequency axis.

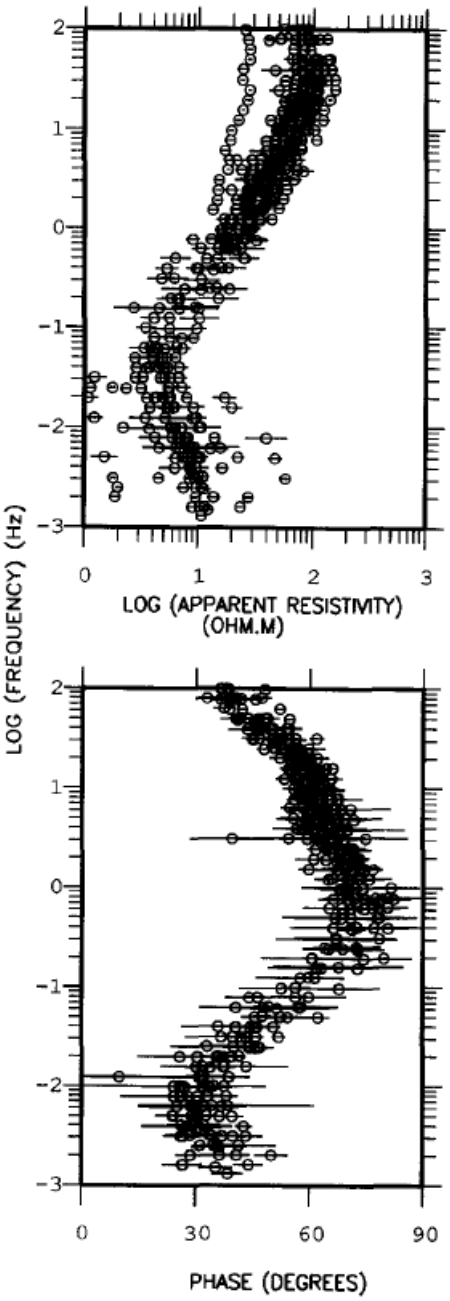

Figure 3. Fig. 3. The 15 sounding curves, in the *XY* component (ρ_{xy}, φ_{xy}), from east-west line 5 (Fig. 2), shown superimposed. Error bars denote I standard error.

Our purpose here is to consider some of the procedures that can be used to provide preliminary assessments of the data characteristics and likely structural influences on the complete data set. As will become apparent later, the data are predominantly one-dimensional and our main attention is directed towards the 1D problem. MT data of the quality shown in Fig. 3 can be viewed as "less than perfect". MT data quality obviously depends (specifically) on the system and processing methods used but it also depends (generally) on the signal/noise environment. The aim of the following discussion is to demonstrate some of the interpretational advantages that can be achieved by the application of the D+ solution to sounding data which are less than perfect.

The D+ solution

The analytic properties that must be obeyed by a physically valid 1D response were considered by Weidelt (1972). The properties are usually described in terms of the complex c-response which is related to apparent resistivity (ρ_a) and phase (φ) as:

$$c(\omega) = (\rho_a/\mu_0\omega)^{1/2} \exp[\,i(\Phi = \pi/2)\,] \qquad (1)$$

Where ω is the angular frequency and μ_0 is the permeability of free space. Weidelt (1972, 1986) discusses a set of inequality constraints which must be upheld by a valid (1D) response. The basis of the constraints lies in the fact that the c-response must always be expressible as an integral over a non-decreasing real function a(λ):

$$c(\omega) = a_0 + \int_0^\infty da(\lambda)/(\lambda + i\omega) \qquad (2)$$

The function a(λ) is the spectral function of the governing field equation. For discontinuous profiles the spectral function must also be discontinuous and will contribute terms of the form $\Delta a_n / (\lambda_n + i\omega)$ where Δa_n (>0) is the magnitude of a jump in a(λ) at location λ_n.

Using equation (2), Parker (1980) provides a complete theory for the existence of valid solutions and constructs the ideal geoelectric profile called the *DPLUS* (D+) solution. This class of solution comprises a finite number of delta functions (layers of zero thickness but finite conductance) separated by perfect insulators. The solution pairs may be obtained using the techniques of quadratic programming, as described by Parker and Whaler (1981).

The existence of non-uniform resistivity structure is detected through the simultaneous (i.e. ρ_a, φ) changes in the gradient of a sounding curve and the D+ solution is no exception. The solution algorithm of Parker and Whaler (1981) provides a single optimum (in terms of misfit) delta function model which may, depending on the misfit achieved, be compatible with the existence of a 1D solution but which will always represent a physically valid response.

As an example consider the sounding data in the *XY* and *YX* components from site 14 shown in Fig. 4. Figure 4a displays the *XY* data and standard errors over the observed bandwidth while Fig. 4b shows the *YX* data plotted within an extended 10 decade bandwidth (discussed later). The D+ algorithm provides solutions which comprise 9 delta functions for each of the two components as listed in

Table 1 and *RMS* misfits (derived from the chi-square statistic) of 0.75 (XY solution) and 0.78 (*YX* solution). These solutions slightly overfit the data in terms of the associated errors.

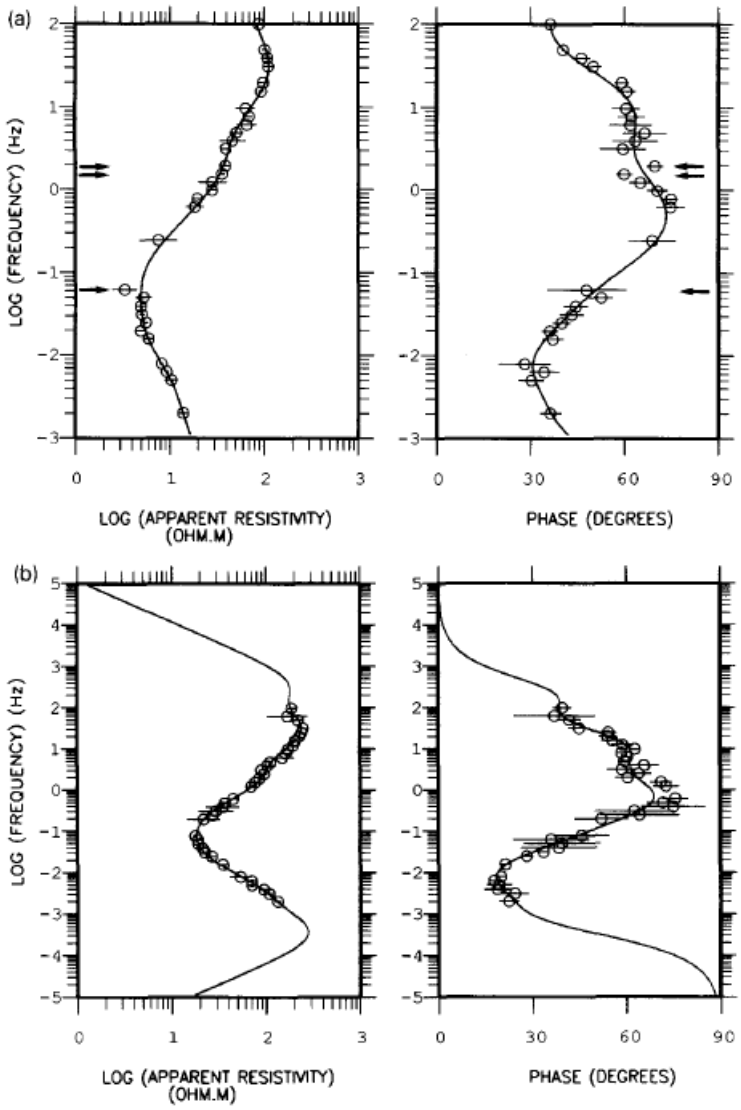

Figure 4. Sounding data from site 14 (discrete symbols) and the responses obtained from the D+ solution (solid lines). (a) *XY* component and (b) *YX* component with the D+ response shown over an extended 10-decade frequency range.

Table 1. Listings of the two D+ solutions for the *XY* and *YX* sounding data at site 14. The *XY* data comprise 30 x 2 frequency estimates and the solution provides a chi-square misfit of 33.7 (RMS error of 0. 75). The *YX* data comprise 37 X 2 frequency estimates and the solution provides a chi-square misfit of 44.7 (RMS error of 0.78). The observed and solution response estimates are compared in Fig. 4. Doublet behaviour can be noted in both solutions at delta functions 4 and 5. Both solutions terminate with a perfect conductor (delta function 9)

Level	*XY* component		*YX* component	
	Depth (m)	Conductance (S)	Depth (m)	Conductance (S)
I	0.0	1.6	0.0	1.0
2	287.5	4.4	443.9	3.3
3	1053.1	59.2	1589.0	35.4

4	2024.1	138.2	3260.8	166.4
5	2210.2	702.8	3651.2	140.5
6	8816.5	573.5	13045.0	164.0
7	20807.0	420.4	52629.0	86.6
8	45675.0	2823.4	192670.0	607.2
9	84550.0		447360.0	

An examination of the D+ solutions, in a like manner, for the entire data set reveals delta function models which are extremely difficult to interpret because of the widespread occurrence of "doublet" behaviour (i.e., the presence of two delta-functions at similar depths), as indicated in Table 1 . Although the models are difficult to interpret directly, the solutions provide the response data shown by the continuous lines in Fig. 4. As the example of Fig. 4 demonstrates, the D+ solution provides a response that contains all the physically valid changes in the gradient of the response while smoothing out the small scale irregularities, particularly in the *paired* estimates of the response. Examples of adequate ρ_a estimates coupled with inadequate ϕ estimates, and vice versa, are shown arrowed in Fig. 4. The essential point is that many of the movements in the observed response, some of which are accommodated by the associated estimates of error, some of which are not, are primarily due to measurement noise rather than, say, 2D or 3D influences. As will be demonstrated later, such "high-order" and unphysical scatter introduces noise in many of the simple transform methods that are used for preliminary interpretation. Such noise contamination becomes particularly acute in methods which require the gradient of the response to be estimated.

For the present data set the D+ response appears to provide a useful set of smoothing and interpolation properties. In addition, the response obtained is both optimum and physically valid. Adequate D+ solutions are also known to exist for data which display 2D and 3D characteristics (Parker, 1983; Beamish, 1986). Larsen (1989) has, in addition, used the D+ solution in connection with an overall data processing strategy to provide smooth and "most one-dimensional" response behaviour. It should also be noted that the D+ solution is an "exact" solution (Parker, 1980). The "observed" standard errors can, however, be associated with the response obtained from the D+ solution if this is considered useful, or indeed meaningful, in the interpretation procedure.

One of the more interesting properties of the D+ solution lies in the *extrapolation* of the response beyond the observed bandwidth. The properties which must be obeyed by a physically valid response at limiting frequencies are discussed by Weidelt (1972) and Parker (1980). Figure 4b compares the observed *YX* component response for site 14 and the D+ solution response extrapolated to cover 10 decades in frequency. The low-frequency behaviour is "damped" by the introduction of a perfect conductor (e.g. delta function 9 in Table 1) which terminates the solution. For these data an at-surface delta function also exists to provide the high-frequency, asymptotic behaviour. The important point to note is that the introduction of artificial model behaviour at limiting frequencies (which cannot be resolved by the data bandwidth anyway) does not distort the optimum gradients within the observed bandwidth.

In determining the D+ solutions for the *XY* component data only 4 soundings (sites 53, 56, 62 and 67) provided *RMS* misfits greater than 3 (i.e., an overall misfit in excess of 3 standard deviations). For the *YX* components this number was reduced to only one (site 63). The vast majority of data provided *RMS* misfits of the order of unity. Having obtained the D+ solution vectors for each sounding, a further advantage is that each solution enables an effectively continuous frequency

response function to be generated. In the case of the present data, which contain significant gaps in individual frequency response curves, the complete array data were resampled using 9 frequency estimates per decade spaced uniformly on a logarithmic frequency scale. It can be appreciated that the resulting 'homogenous' data set provides significant advantages in many of the subsequent processing procedures that can be applied to array data.

In order to demonstrate the advantages of the D+ processed data set, both raw and processed data are now used in several preliminary processing procedures. The sounding data obtained across east-west line 5 are used for illustrative purposes.

Assessments of static distortion

A recent review of the subject of static distortion in MT is provided by Jiracek (1990). The presence of static distortion due to near-surface galvanic effects above an otherwise 1D structure would be detected by strictly parallel behaviour between the measured off-diagonal apparent resistivity sounding data. The parallel behaviour would be maintained across the entire sounding bandwidth (unless super-high-frequency estimates are available) and the phase data would be identical. Any 2D or 3D structural contributions superimposed on this simple model are likely to introduce inductive (frequency-dependent) behaviour in the relative attitudes of the two off-diagonal components. As a general rule, the increase of the sounding volume that accompanies decreasing frequency is likely to provide a greater probability for inductive effects to contribute to the sounding data. Since the assessment of static distortion is such an important stage of the interpretation procedure, our ability to quantify "parallel behaviour" as a function of frequency becomes of critical importance.

Qualitative assessments

In many cases assessments of parallel behaviour have been undertaken in a qualitative manner using presentations of the apparent resistivity sounding data in the usual logarithmic coordinates. The raw and processed *YX* component data from the 15 soundings across line 5 are shown superimposed in Fig. 5a, b. The use of the continuous sounding presentation in Fig. 5 arises from the aim of detecting parallel behaviour and errors are omitted for clarity. Although only first-order behaviour can readily be identified from bulk presentations of this kind, some departures from the simple parallel behaviour associated with static distortion can be observed. In order to understand such departures the observational errors must be taken into account. Typical data errors (e.g. Fig. 3) cannot account for the range of values in apparent resistivity (i.e., of the order of 1 decade) observed across the 15 soundings sites in the *YX* component. The range of values obtained for the D+ processed phase data (Fig. 5b) across the 15 sites is 9 degrees at 100 Hz and 12 degrees at 0.01 Hz. if observational errors of the order of 5 degrees are allowed for (e.g. Fig. 3) then the *YX* component phase data cross line 5 could be expected to arise from the same structural model.

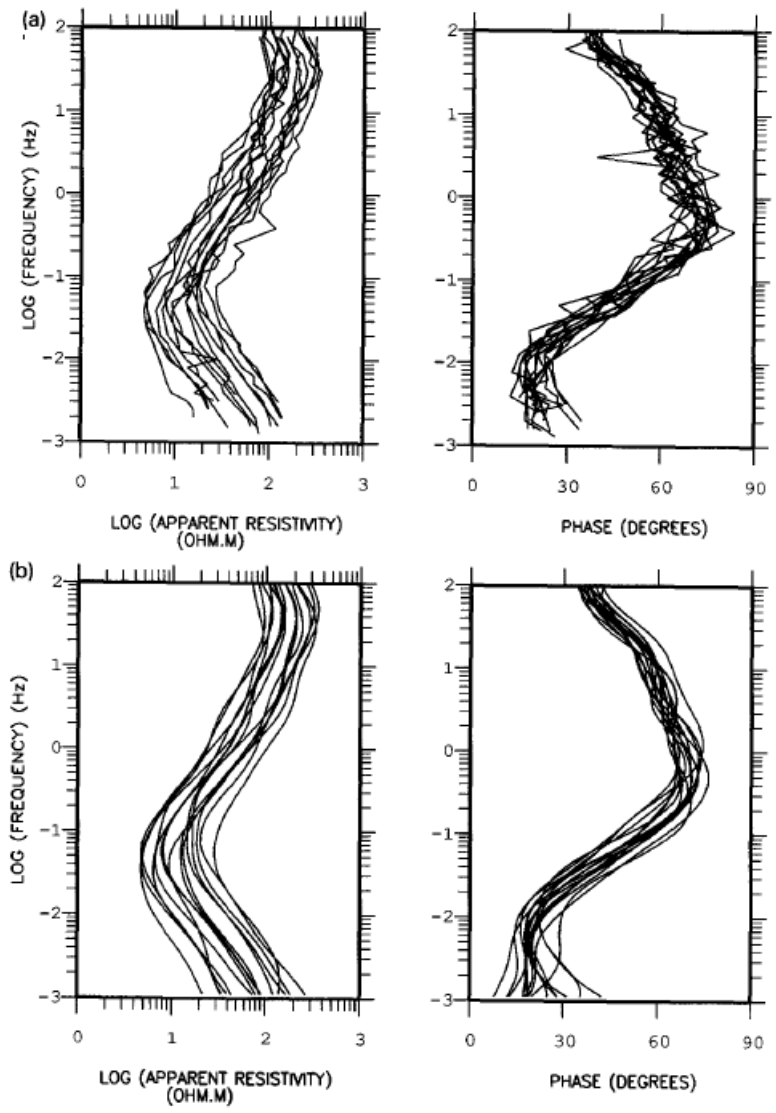

Figure 5. The 15 sounding curves in the *YX* component *(ρ_{yx}, φ_{yx})* from east-west line 5. (a)Raw data with errors omitted for clarity, and (b)equivalent data processed using the D+ solution.

Quantitative assessments

It should be appreciated that presentation of apparent resistivity on a logarithmic scale, such as those of Fig. 5, may mask important localised frequency-dependent effects. To quantify the degree of parallel and frequency-independent behaviour it is suggested that the apparent resistivity sounding data are best assessed by forming the simple anisotropy ratio, which is the ratio between the observed off-diagonal apparent resistivity curves (e.g. ρ_{xy}, ρ_{yx}). Parallel behaviour between sites can also be assessed using ratios such as ρ_{xy}/ρ_{yx} for example. Since the calculation of the anisotropy ratio involves a quotient the result can be subjected to considerable scatter (with frequency) introduced by errors in one or both apparent resistivity values. This was found to be the case when anisotropy ratios were calculated using the raw data samples such as those of Figs. 3 and 5a. The D+ processed sounding data, since they have been subjected to a "regularisation" procedure, provided a much more consistent set of results, as shown in Fig. 6. This figure shows the anisotropy ratios, on

a linear scale, in cross-sectional form for the 14 sites along an east-west profile (line 5, sounding 10 omitted for clarity) for the 5 decade sounding bandwidth.

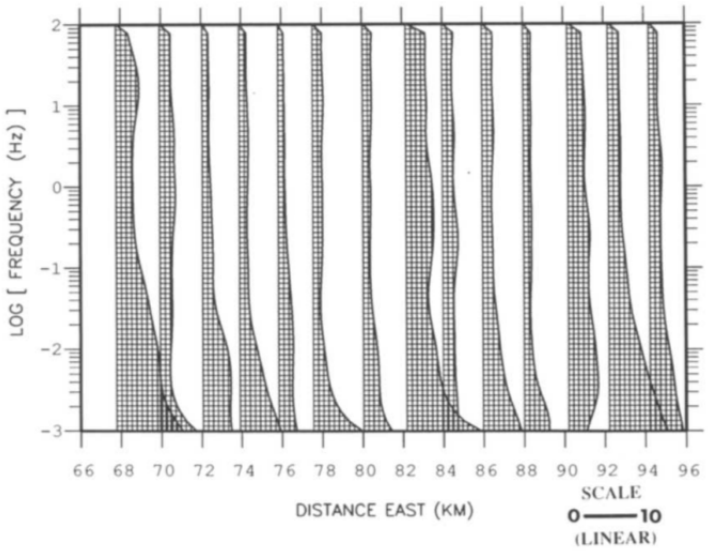

Figure 6. Anisotropy ratios (ρ_{yx}/ρ_{xy}) for the D+ processed data from line 5 (14 locations, data from site 10 omitted for clarity). Results plotted on a linear scale (see scale bar) , as a function of frequency (logarithmic scale) and position . The zero position of the anisotropy ratio is located at the grid easting of each sounding.

The majority of soundings display anisotropy ratios in the range 1 to 3 and the lack of any significant movement with frequency indicates parallel behaviour over the first (upper) 3 frequency decades. This was found to be the case for the majority of all the array soundings. Soundings which form "outliers" can readily be identified such as soundings 1 and 8 in Fig. 6. These soundings also appear to possess anisotropy ratios with a greater degree of frequency dependence. At lower frequencies, distinct frequency dependence can be observed whose onset occurs at frequencies in the interval 0.1 to 0.01 Hz. At these low frequencies the sounding curves begin to diverge. The "degree of divergence" as measured by the anisotropy ratios appears to be spatially variable and so it appears difficult to attribute such behaviour to large scale (e.g. regional) structural contributions.

The frequency range over which parallel behaviour is observed can be further used to summarise the magnitude of the static distortion effects observed across the array. Figure 7 shows the values of the anisotropy ratio calculated as an average over the frequency interval from 100 to 0.1 Hz for the whole data set. An artificial ratio limit of 10 was applied since only 3 soundings display excessive (order of magnitude) distortion effects. The three soundings at sites 40, 55 and 63 provided averaged anisotropy ratios of 17, 19 and 14, respectively. The spatially "random" nature of the soundings possessing high anisotropy ratios together with the predominance of values less than 4 can be noted in the results obtained. Figure 7, used in conjunction with the type of frequency dependent information shown in Fig. 6, effectively illustrates the form and magnitude of the static distortion influences on the data set. Figure 7, in particular, offers a schematic reference when considering the most appropriate processing method for the suppression of the distortion effects encountered.

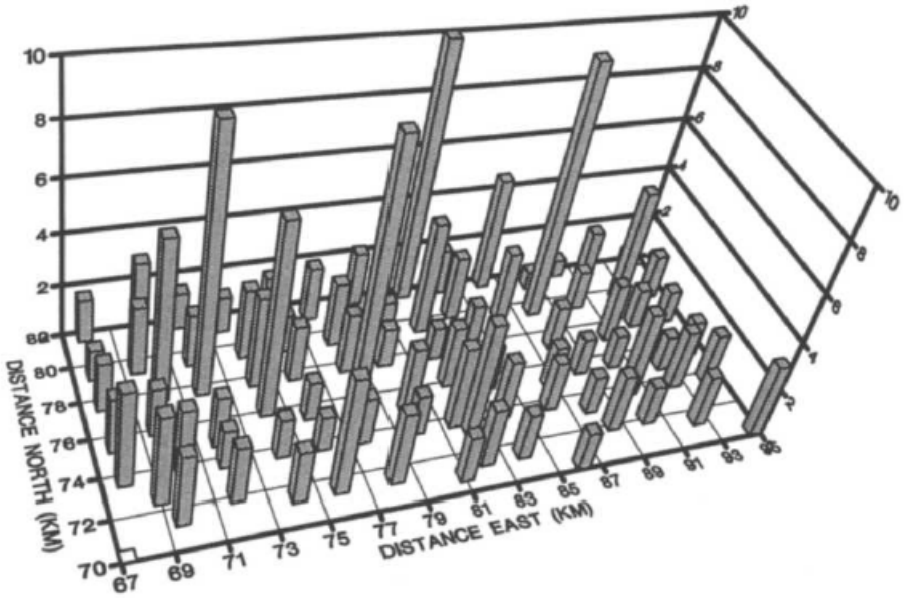

Figure 7. Average anisotropy ratios (ρ_{yx}/ρ_{xy}), calculated as the average value over the frequency interval from 100 to 0.1 Hz, over which a high degree of parallel behaviour is observed (see Fig. 6). The average is plotted on a linear scale (0 to 10) as a function of sounding location for all 84 sites.

Spatial averages

Since the D+ solution provides optimum smoothing, the processed sounding data contain only physically valid movements (subject to the assumption of one-dimensionality). The noise reduction inherent in the processing is valuable when spatial averages across a number of sounding curves are required (e.g. to suppress distortion effects). This becomes particularly important when only small numbers of data are available. As an example Fig. 8 displays the raw *XY* component data at the four sites - 7, 8, 9 and 10 (line 5, Fig. 2). The irregular frequency sampling can be noted. The D+ solution response data for the 4 soundings were used to form an average, in this case a median, sounding curve which is shown as the solid line in Fig. 8. The data statistics are treated in the logarithmic domain in apparent resistivity and in the linear domain for phase. Using Fig. 8 it can be appreciated that the D+ average (i.e., the average of the 4 individual D+ soundings) contains some important and diagnostic changes in gradient which may not be apparent when the statistics of the raw sounding curves are examined.

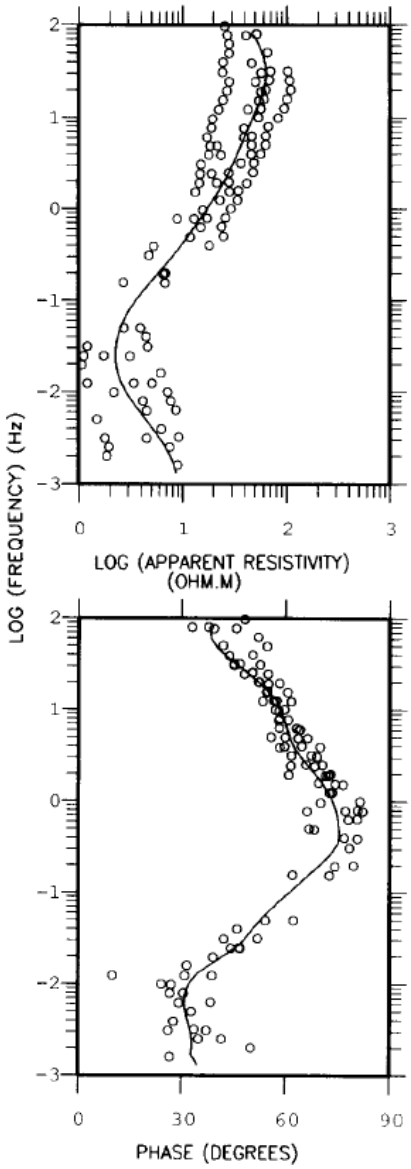

Figure 8. Raw sounding data from 4 sites (7, 8, 9 and I 0, from line 5) shown as discrete symbols. Error bars are omitted for clarity. The D+ average result is shown by the solid line.

In the case of the present data set, spatial averages (again median values) were determined from the D+ processed sounding data to reveal an interesting data characteristic. Spatial averages were formed using the data contained across each of the 6 east-west lines of Fig. 2 (about 14 soundings per line). The formation of "line-averages" is clearly not optimum, in a spatial sense, for array data but is adequate for the illustrative purposes here. The median sounding curves in individual *(XY, YX)* components for the 6 lines are shown in Fig. 9. The *XY* component data are displayed as continuous lines and the *YX* component data as discrete symbols. In Fig. 9 it can be seen that in each component the average sounding is a curve whose apparent resistivity appears to undergo a moderate amount of parallel shift across the ensemble of 6 estimates, the phase remaining substantially the same. Thus for each sounding component it appears that the spatial average value of apparent resistivity is a function of the levels of static distortion encountered in the ensemble used. Such effects appear to be essentially random across the array. A *systematic* effect is observed, however, in the separation of the XY and *YX* component averages in apparent resistivity while the phase values remain similar

until the lower frequency portion of the bandwidth. The effect observed appears to be a random level of static distortion in individual components and a systematic (i.e. spatially consistent) distortion offset between components. Using the phase data in Fig. 9 as a control, this "model" of distortion characteristics appears broadly correct until departures are evident at frequencies below 0.1 Hz.

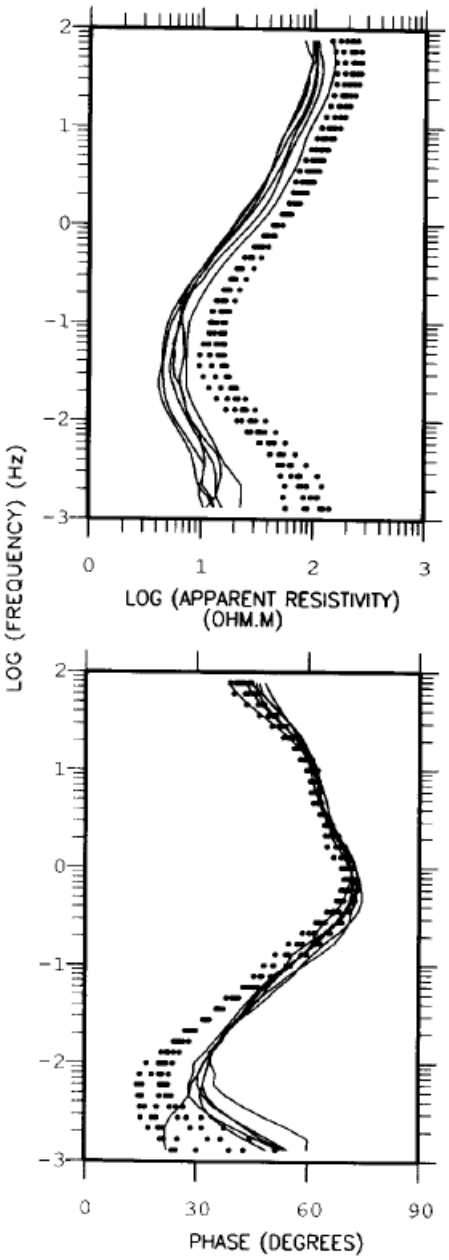

Figure 9. D+ processed sounding data averaged over the 6 east-west lines of Figure 2 to produce 6 sounding curves in each of 2 components. The *XY* component data $(\rho_{xy}, \varphi_{xy})$ are shown by the solid lines and the *YX* component data $(\rho_{yx}, \varphi_{yx})$ are shown by the discrete symbols.

The data characteristics suggest a structural model often associated with large-scale sedimentary basins. The conceptual model consists of a non-uniform thin sheet above an earth in which a 1D model is valid down to a minimum frequency.

Approximate l D transforms

A number of approximate transforms can be applied directly to sounding data to obtain a first approximation to the resistivity profiles at individual locations. Clearly the transforms are most effective on data which can be considered l D. The transforms are "continuous" in the sense that they operate directly on the sounding data. Such transforms always represent smoothed approximations to the "true" resistivity structure. Schmucker (1987) provides details and relationships between the Niblett-Bostick, the Molochnov and the *p*-z** transforms that can be used. Before discussing the common Niblett-Bostick (N-B) transform, it is worth noting at this point that the "exact" D+ solution can also be transformed into an approximate and more conventional resistivity/depth profile.

An approximate transform for the D+ solution

As discussed previously the D+ solution consists of a number of delta functions of given conductance at fixed and increasing depths. This depth profile can be converted to a depth-integrated conductance (S) down to a depth *z* as:

$$S(z) = \int_0^z \sigma(z')\, dz'$$

This is a completely general formula for any vertical conductivity profile ρ(z). In the case of the D+ model, contributions to S(z) only arise at the depths of the delta functions. The "average" resistivity (ρ^a) at each incremental delta function depth may then be calculated as $\rho^a = z_i/S_i$ (e.g. Jain, 1966). This procedure was applied to the *XY* and *YX* component solutions shown in Table 1 for delta functions 2 to 7. The results are shown in log/log scale in Fig. 10. It can be noted that the approximate pro files obtained indicate a resistive/conductive/ resistive sequence with increasing depth. Equally important is the observation that there exists a parallel offset between the resistivity profiles of the two components.

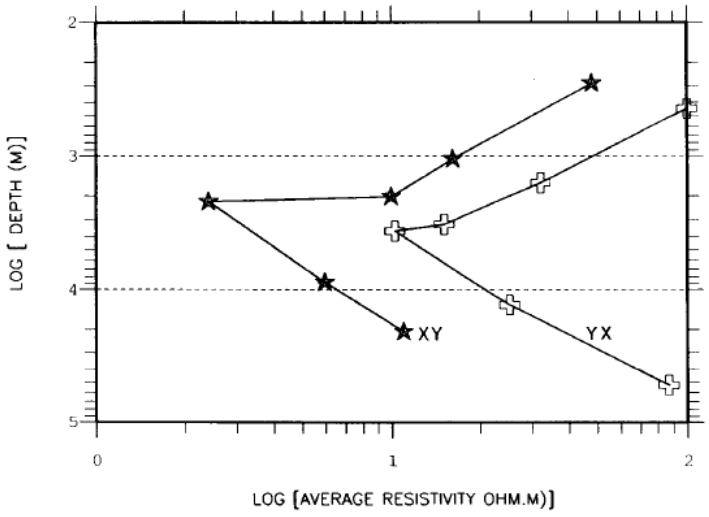

Figure 10. D+ solution model transformed to an approximate resistivity/depth profile, using data of site 14. Profiles for both *XY* and *YX* component data are shown.

Following the assessment of the static distortion characteristics of the data set it should be apparent that *all* the methods of translating the sounding data to a resistivity depth profile will produce characteristic parallel offsets between the *XY* and *YX* profiles when the results are plotted in the usual log/log coordinates (Larsen, 1977). The degree of offset will be a function of the anisotropy ratios discussed previously.

The N-B transform

As indicated in Fig. 10, a three-layer resistive/ conductive/ resistive (half-space) model provides the essential first-order features found in the sounding data across the whole array. A representative three-layer model consisting of a basalt layer (ρ_1 = 100 Ω·m) of depth 2 km and a thin sedimentary layer of thickness 1 km (ρ_2 =5 Ω·m) underlain by an electrical basement of resistivity (ρ_3 =200 Ω ·m) is shown in Fig. 11a. Figure 11b is discussed later. The N-B transform of the response of this model (high-frequency limit 100 Hz) is shown alongside. The usual asymptotic behaviour of the transform is very evident. It can be seen that only the resistivity of the basalt layer together with the transition depth to the conductive layer is adequately "resolved". The transform provides virtually no interpretation control with regard to the thickness, and therefore depth to base, of the sedimentary layer. The primary use of the transform, as discussed here, can only be in relation to the resistivity and depth of the basalt layer.

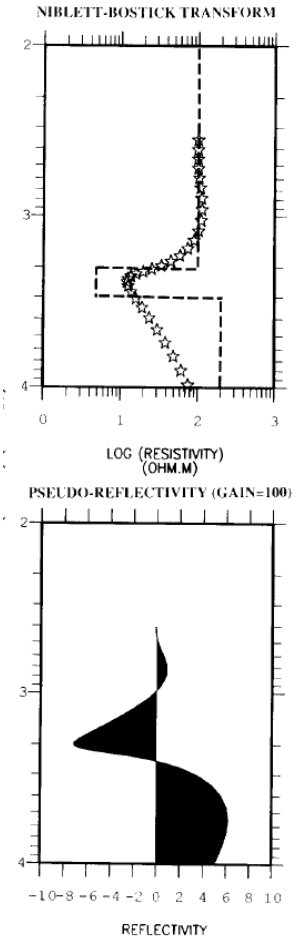

Figure 11. Three-layer forward model, shown as a dashed line in left diagram compared with results of two approximate transform methods which use the response of the model (top), Niblett-Bostick transform shown as discrete symbols and (bottom) the pseudo-reflectivity profile.

The N-B transforms of the raw and D+ processed sounding data, in both *XY and YX* components, at sites 1 and 14 are shown in Fig. 12. Raw data transforms are denoted by discrete symbols and processed data transforms by continuous lines. The "adequacy" of the three-layer forward model can be assessed by comparing Figures 11a and 12. The comparison of the raw and processed data transforms in Fig. 12 illustrates several points. The first is that the raw data transforms contain inconsistent and unphysical scatter in that the conditions for validity (e.g. Weidelt, 1972) require, for example, a transform depth which decreases monotonically with decreasing frequency. The D+ processed data transforms will necessarily satisfy all known conditions for physical validity. The second point is that the processed data far more clearly reveal "structure" in the upper portion of the section (i.e., at depths prior to the minimum resistivity) that is consistent, to a certain degree, between different components and between the two sites. This structure is, in fact, genuine and corresponds to a "two-layer" sequence prior to the most conductive sedimentary formation. The third point is that due to unequal frequency sampling, the raw transform estimates may not exist at 'critical' frequencies where turning points exist in the resistivity profile (e.g. site 1, Fig. 12). The interpolation properties of the processed data then become important.

Pseudo-reflectivity

The subject of imaging reflectivity in MT interpretation has been discussed by a number of authors and is reviewed by Oldenburg (l 990) . One approach follows that used in reflection seismology where reflection seismograms are processed to produce a stacked section across which correlatable events are interpreted as reflections from an interface. Inversion would then follow as a subsequent processing step. Here we consider the reverse approach (e.g. Shoemaker et al., 1989), in which the results of data inversion (here a l D resistivity/ depth profile) can be used to form reflection coefficients. The essential ingredient in both approaches is a presentation that permits easy interpretation of lateral correlation.

A simple method is to use the definition of reflection coefficients that arises due to the boundary conditions that exist between different electrical media in a 1D multi-layered Earth (Cagniard, 1953). The MT reflection coefficients (r_j) that arise between two layers of resistivities ρ_j and ρ_{j+1} are defined as:

$$r_j = \frac{\sqrt{\rho_{j+1}} - \sqrt{\rho_j}}{\sqrt{\rho_{j+1}} + \sqrt{\rho_j}} \qquad (3)$$

Obviously such instantaneous reflection coefficients may be obtained using any available resistivity profile. Since they are intended for use in relation to discontinuous media their application using continuous (either approximate, as here, or exact) resistivity/depth profiles is not immediately evident. They do, however, seem to offer certain interpretational advantages when applied to direct transform results as discussed below. The most obvious "benefit" is that the interpretation problem reduces from being a problem in joint resistivity and depth to one consisting primarily of depth dependent behaviour.

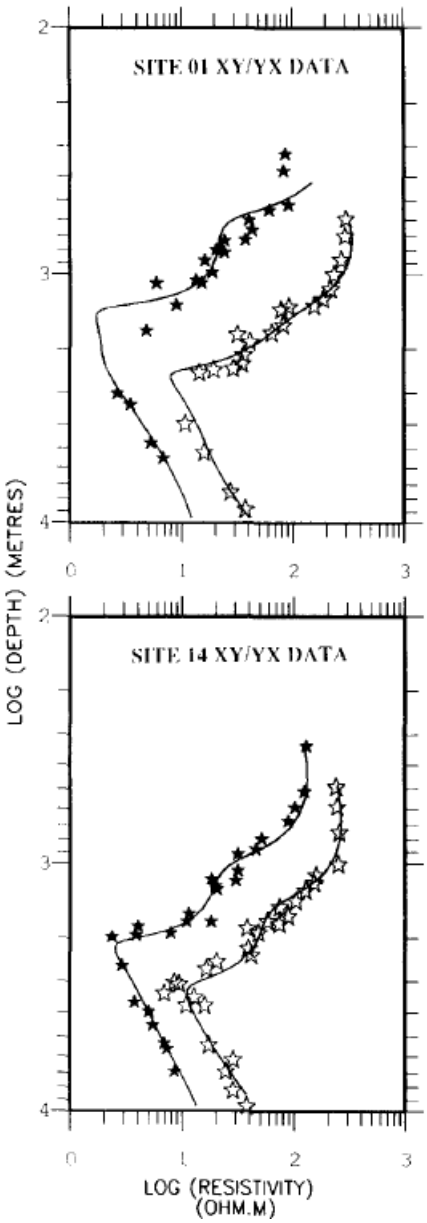

Figure 12. Niblett-Bostick transforms obtained using the raw sounding data (discrete symbols) and the D+ processed data (solid lines). Data from sites 1 and 14. The *XY* component data are displayed as the solid symbols and the *YX* component data as the open symbols.

The N-B transform assigns a resistivity by taking frequency derivatives of the observed response into account (Schmucker, 1987). When equation (3) is applied to such a transform, a depth derivative is obtained. This makes the two stage procedure extremely sensitive to the quality and physical validity of the sounding data used. The N-B transform of our three-layer forward model was shown in Fig. 11a. The sounding data associated with this model obviously represent a no-noise, physically valid case. The reflectivity coefficients obtained from these data are shown in Fig. 11b. The sensitivity of equation (3) to the depth profile on which it is applied can be seen by comparing Figs. 11a,b. The initial set of small positive reflection coefficients are generated by the inherent (but false) initial oscillation in the N-B transform. The maximum in the depth derivative of the transform provides the maximum (negative) reflectivity at the depth of the layer 1/layer 2 transition (at 2 km). The subsequent transition from negative to positive reflection coefficients (i.e. zero reflectivity) occurs

halfway through the second (conductive) layer. Simple forward modelling of other three-layer models of this type indicates that such attributes are provided by the procedure down to quite small resistivity contrasts (e.g. 2) between the first and second layers. It should be apparent that the presentation in terms of reflection coefficients offers an "amplification" of the frequency characteristics of the sounding data. It should also be noted that the presentation in terms of reflection coefficients will suffer the same degree of approximation (and equivalent resolution attributes) as the resistivity profile from which it is derived.

The magnitude of the reflection coefficients, as determined here, will depend on the frequency resolution of the original sounding data. Using a seismic analogy the MT response function is sampling a layered system with unequal delay. This is not a practical problem if all the sounding data are sampled adequately and uniformly in frequency and the same gain factors are applied to all reflection coefficients. These aspects of the procedure together with the fact that only an approximate and continuous transform is used suggest that the presentation should be referred to as pseudo-reflectivity.

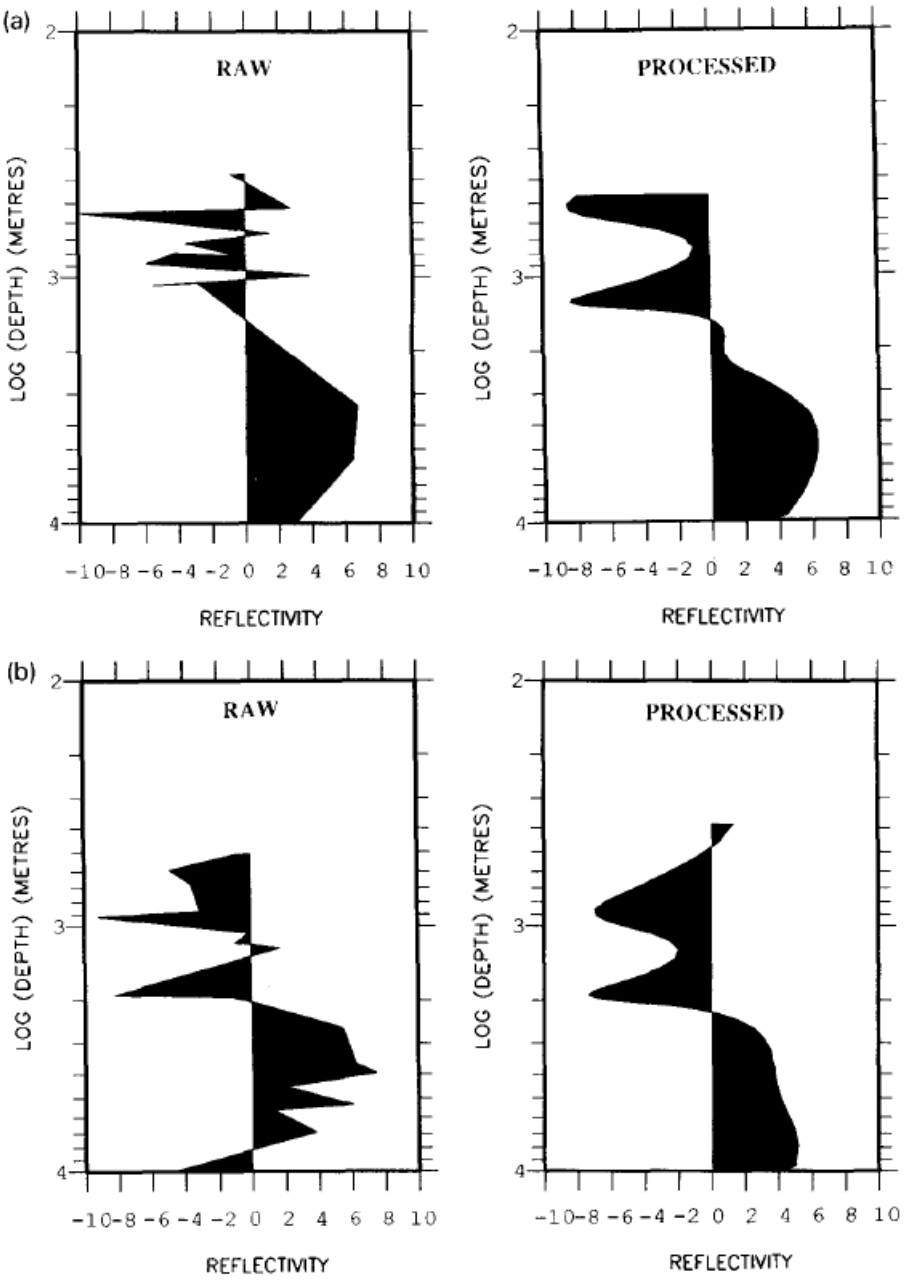

Figure 13. Pseudo-reflectivity profiles (gain = 100) obtained using the raw and D+ processed data at site I (a) and 14 (b) Only the *XY* component data are used.

The pseudo-reflectivity profiles determined using the raw and processed *XY* component data at sites 1 and 14 are shown in Fig. 13. The results can be compared with the equivalent N-B transform results shown in Fig. 12. It seems very evident that the raw sounding data are totally inadequate, in terms of unequal frequency sampling and unphysical scatter, with regard to such a data-sensitive form of presentation. The processed data appear however to offer scope for an examination of the horizontal continuity of the reflections associated with the basalt layer, the base of this layer and the depth location of zero reflectivity. Obviously the main use for this form of presentation is in relation to lateral correlations to facilitate the interpretation of the continuity of structural horizons. When, as is the case here, the measured data are influenced by static distortion, the depth information will be corrupt and both assessment and suppression of distortion effects must be carried out prior to such presentations. Distortion correction techniques have been recently reviewed by Jiracek (1990)

and a number of these techniques, applied to the present array data, will be discussed elsewhere. As an illustration only, Fig. 14 provides an example of the utility of the pseudo-reflectivity method of presentation when applied to the data from line 5 which have been processed to suppress the influences of static distortion.

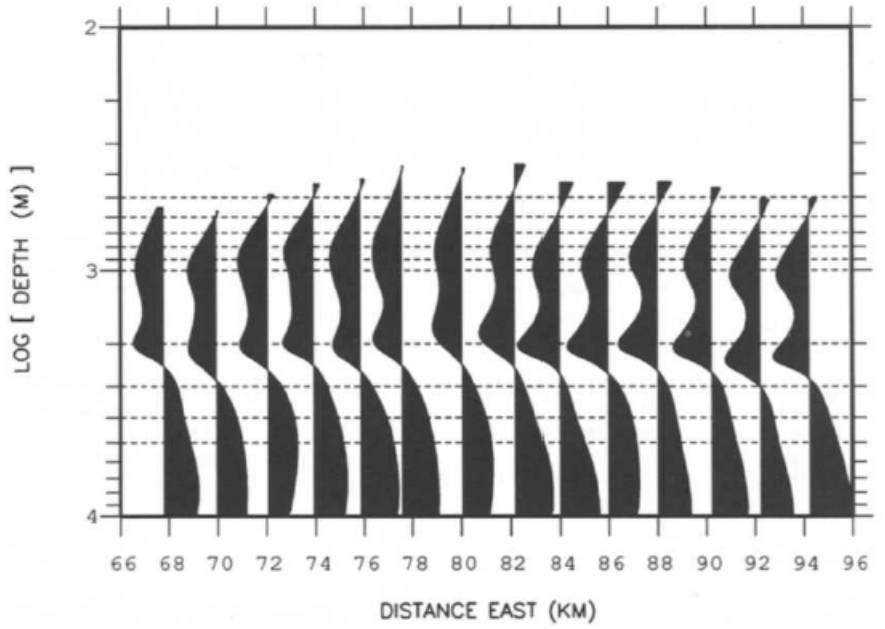

Figure 14. Example of pseudo-reflectivity presentation of D+ processed sounding data from east-west line 5 which have been further processed to suppress the influences of static distortion.

Conclusions

The D+ processing procedure provides a method of ensuring a physically-valid (minimum-phase) response from data which have 1D response characteristics. The technique, since it is an optimum procedure, appears to offer advantages over alternative (ad-hoc) methods. In the case of the present array data, the application of D+ processing resulted in a much improved, homogenous (in frequency) and consistent (physically valid) data set. The interpretational advantages of the processing procedure have been illustrated using anisotropy ratios, spatial averaging and simple transform methods which recover resistivity/depth and reflectivity profiles.

Acknowledgements

We are grateful to Bob Parker for providing the original coding of his algorithms which have provided such valuable insights into our data. This paper is published with the approval of the Director, British Geological Survey (NERC).

References

Beamish, D., 1986. Geoelectric structural dimensions: methods of estimation old and new. Geophysics, 51 : 1298-1309.

Cagniard, L., 1953. Basic theory of the magnetotelluric method of geophysical prospecting. Geophysics, 18: 605-635.

Fischer, G. and Schnegg, P.A., 1980. The dispersion relations of the magnetotelluric response and their incidence on the inversion problem. Geophys. J. R. Astr. Soc., 62: 661-673.

Jain, S., 1966. A simple method of magnetotelluric interpretation. Geophys. Prospect., 14: 143-148.

Jiracek, G.R., 1990. Near-surface and topographic distortions in electromagnetic induction. Surv. Geophys., 1 1 : 163-203.

Jiracek, G.R., Curtis, J.H., Ramirez, J., Martinez, M. and Romo, J., 1989. Two-dimensional magnetotelluric inversion of the EMSLAB Lincoln line. J. Geophys. Res., 94: 14145-14151.

Jones, A.G., Chave, A.D., Egbert, G., Auld, D. and Bahr, K., 1989. A comparison of techniques for magnetotelluric response function estimation. J.; Geophys. Res., 94: 14,201-14,213.

Larsen, J.C., 1977. Removal of local surface conductivity effects from low frequency mantle response curves. Acta Geodaet. Geophys. Montanist. Acad. Sci. Hung., 12: 183-186.

Larsen, J.C., 1989. Transfer functions: smooth robust estimates by least-squares and remote reference methods. Geophys. J. Int., 99: 645-6633.

Morrison, H.F., Nichols, E.A., Torres-Verdin, C., Booker, J.R. and Constable, S.C., 1990. Comparison of magnetotelluric inversion techniques on a mineral prospect in Nevada. 60th Annual Meeting, SEG, Expanded Abstracts, San Francisco, pp. 516-519.

Oldenburg, D., 1990. Inversion of electromagnetic data: an overview of techniques. Surv. Geophys., 11: 231-270.

Park, S.K., Biasi, G.P., Mackie, R.L. and Madden, T.R., I 991. Magnetotelluric evidence for crustal suture zones bounding the southern Great Valley, California. J. Geophys. Res., 96: 353-376.

Parker, R.L., 1980. The inverse problem of electromagnetic induction: existence and construction of solutions based on incomplete data. J. Geophys. Res., 85: 4421-4428.

Parker, R.L., 1983. The magnetotelluric inverse problem. Geophys. Surv., 6: 5-25.

Parker, R.L. and Whaler, K.A., 1981. Numerical methods for establishing solutions to the inverse problem of electromagnetic induction. J. Geophys. Res., 86: 9574- 9584.

Schmucker, U., 1987. Substitute conductors for electromagnetic response estimates. PAGEOPH., 125: 341- 367.

Shoemaker, C.L., Shoham, Y. and Hockey, R.L., 1989. Calibration case study of natural source electromagnetic array data recorded over a well in Oregon. Proc. IEEE, 77: 334-337.

Stanley, W.D., Saad, A.R. and Ohofugi, W., 1985. Regional magnetotelluric surveys in hydrocarbon exploration, Parana Basin, Brazil. Bull. A.A.P.G., 69: 346- 360.

Tzanis, A. and Beamish, D., 1989. A high-resolution spectral study of audiomagnetotelluric data and noise interactions. Geophys. J., 97: 557-572.

Weidelt, P., 1972. The inverse problem of geomagnetic induction. Z. Geophys., 38: 257-289.

Weidelt, P., 1986. Discrete frequency inequalities for magnetotelluric impedances of one-dimensional conductors. J. Geophys., 59: 171-176.

Young, C.T. and Kitchen, M.R., 1989. A magnetotelluric transect in the Oregon coast range. J. Geophys. Res., 94: 14,185-14,193.

Zalan, P.V., Conceiao, J.C.J., Wolff, S., Astolfi, M.A.M., Vieira, V.T., Santos Neto, E.V., Cerqueira, J.R., Zanoto, O.A. and Paumer, M.L., 1986. Analise da Bacia do Parana. GT-Os-009/85, PETROBRAS/DEPEX, Rio de Janeiro.